4

NANOSTRUCTURED POLYMERIC NANOREACTORS FOR METAL NANOPARTICLE FORMATION

L. M. Bronstein

Department of Chemistry, Indiana University, Bloomington, Indiana

1. INTRODUCTION

Formation of metal nanoparticles in a polymer matrix became a popular tool for design of new metal–polymer nanocomposites, the properties of which can be greatly altered compared to those of pure polymers [1–4]. Incorporation of nanoparticles into a polymeric system may impart magnetic, semiconductor, catalytic, or sensing properties, depending on the kind of nanoparticles, formed inside a polymer, and nanoparticle characteristics. To obtain metal–polymer nanocomposites with well-defined and well-reproducible properties, one should carry out a subtle control over nanoparticle growth, particle size distribution, and particle-interface interactions. These are key issues to the desired properties and targeted applications of polymeric materials. Narrow particle size distribution is especially crucial, since optical, magnetic, sensing, and even catalytic properties strongly depend on the precise control over particle size. One of the prominent ways to control nanoparticle size and morphology is to employ functional polymeric nanostructures with well-defined interfaces [5–7]. These interfaces can be generated via hydrophobic–hydrophilic microphase separation; or, due to nanopores or nanocavities, they can be formed within a

Metal-Polymer Nanocomposites, Edited by Luigi Nicolais and Gianfranco Carotenuto
ISBN 0-471-47131-3 Copyright © 2005 John Wiley & Sons, Inc.

SOFTbank E-Book Center Tehran, Phone: 66403879,66493070 For Educational Use.

polymer during synthesis. The presence of functional groups able to interact with metal compounds allows incorporation of metal species into the functional nanophase, while subsequent reduction or thermal (or other) treatment results in nanoparticle formation within this restricted area. The characteristics of the functional nanophase, metal compound loading, type of reducing agent, and other parameters are responsible for metal nanoparticle and metal–polymer nanocomposite characteristics. This chapter describes our major accomplishments in the field of metal–polymer nanocomposites, illustrating synthetic approaches, structural characterization, and properties. Comprehensive review articles describing "Nanoparticles in Nanostructured Polymers" and "Polymer Colloids and Their Metallation" are presented in the *Encyclopedia of Nanoscience and Nanotechnology* (American Scientific Publishers, 2004) and the *Dekker Encyclopedia of Nanoscience and Nanotechnology* (Marcel Dekker, 2004). In this chapter, all nanostructured polymeric systems are divided into two large groups—solid or heterogeneous (insoluble in any media) and soluble or microheterogeneous (colloidally soluble)—and will be discussed in separate sections.

2. SOLID POLYMER NANOSTRUCTURES

Among solid polymer nanostructures, two types of systems will be described: (a) complexes of polyelectrolyte gels with surfactants and (b) crosslinked polymers containing nanopores or nanocavities.

2.1. Polyelectrolyte Gel–Surfactant Complexes

Polyelectrolyte gel–surfactant complexes are formed when a polyelectrolyte gel is placed in the solution of oppositely charged surfactants. Surfactant molecules easily penetrate a gel due to hydrophobic interactions and form complexes with the polyelectrolyte charged groups. At the same time, surfactant molecules self-assemble within the gel, and their ordering even exceeds the ordering of surfactants in solutions, as was reported in a number of publications [8–12]. Since a polyelectrolyte gel–surfactant complex contains counterions in well-ordered surfactant areas within a weakly crosslinked gel, these counterions can be replaced with ions of interest (transition metal ions). The subsequent treatment (reduction, thermolysis, photolysis, etc.) should lead to formation of nanoparticles in a well-ordered nanostructured medium. Indeed, metal ions are absorbed by polyelectrolyte gel–surfactant complexes when these ions are oppositely charged toward polyelectrolyte charged groups [13–16]. However, incorporation of the ions does not destroy the surfactant ordering: Metal compounds form

SOFTbank E-Book Center Tehran, Phone: 66403879,66493070 For Educational Use.

clusters located between charged groups of a polyelectrolyte chain and surfactant head groups. During further reduction, these clusters play the role of nuclei for metal nanoparticle formation.

The use of small-angle X-ray scattering (SAXS) and anomalous SAXS (ASAXS) [15] allowed us to quantitatively characterize the influence of the type of the reducing agent and of the structure of the metal compound on size distributions of Pt nanoparticles formed in polyelectrolyte gel–surfactant complexes. We studied three collapsed gel–surfactant complexes: a cationic gel of polydiallyldimethylammonium chloride (PDADMACl) with two anionic surfactants, sodium dodecyl sulfate (SDS) and sodium dodecylbenzene sulfonate (SDBS); and an anionic gel of poly(methacrylic acid) with a cationic surfactant, cetylpyridinium chloride (PMA/CPC). For all the cationic gel–anionic surfactant complexes, the sluggish reducing agent ($N_2H_4 \cdot H_2O$) leads to much larger nanoparticles than does the fast reducing agent ($NaBH_4$), yet the metal compound structure plays a crucial role in nanoparticle formation. The particles obtained from the planar $PtCl_4^{2-}$ ions are smaller (the mean radius of a small particle fraction is about 1 nm) and have a narrower size distribution; moreover, particles larger than 15–20 nm are absent (Figure 4.1). In contrast, the octahedral $PtCl_6^{2-}$ ion-based materials yield larger particles. In so doing, the gel–surfactant complex derived from H_2PtCl_6 (low pH) yields particles with the radii up to 40 nm. Even larger particles (with the radii up to 80 nm) are formed in the anionic gel–cationic surfactant complex PMA/CPC where the particle growth is not controlled by the internal gel structure [15]. Presumably, the formation of larger particles in the PDADMACl–SDS system from $PtCl_6^{2-}$ ions than from $PtCl_4^{2-}$ ions is due to formation of larger precursor (salt) clusters from ions with octahedral geometry.

Analysis of the Bragg peaks in the scattering data permitted us to also quantitatively characterize the ordering in the gel–surfactant complexes. In Table 4.1 one can see the structural parameters characterizing the internal order in the collapsed polyelectrolyte gel–surfactant complexes calculated from the Bragg peaks in the SAXS and ASAXS profiles. The mean long-range order dimension L estimating the size of quasi-crystalline zones in the sample, as well as the radius of interaction r_m yielding maximum separation between spatially correlated structural motifs, should increase with increasing order in the system. In contrast, the relative mean square deviation of the distance between the neighboring periodic motifs $\Delta/\bar{d}$ (degree of disorder) should decrease if the system becomes more ordered, while the Bragg peaks nearly disappear if $\Delta/\bar{d} > 0.25$.

A surprising result was obtained for both cationic gel–anionic surfactant systems: The metal-containing samples appear not less ordered than the initial polyelectrolyte gel–surfactant complexes despite the diminished amplitudes of the peaks. For the PDADMACl–SDBS system, the average distance between

SOFTbank E-Book Center Tehran, Phone: 66403879,66493070 For Educational Use.

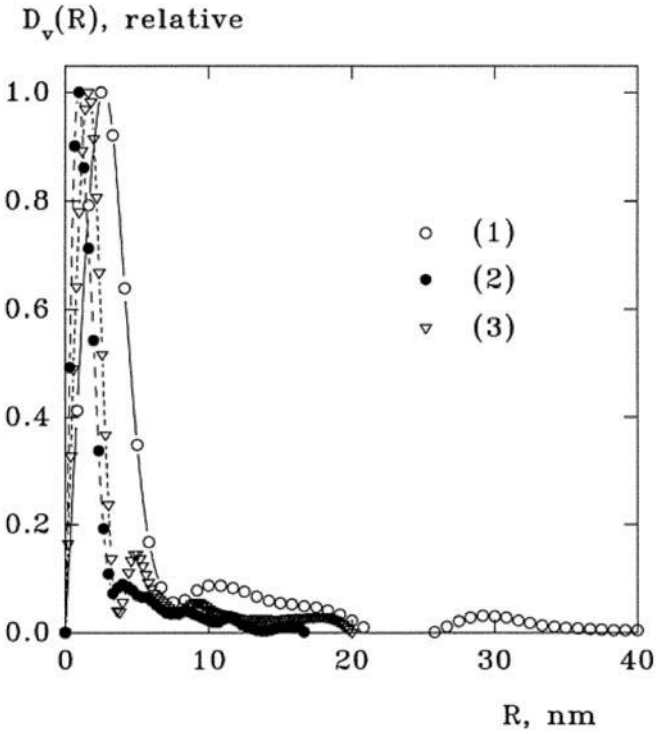

Figure 4.1. Volume distribution functions evaluated by GNOM for the PDADMACl–SDS gel containing Pt nanoparticles derived from H_2PtCl_6 (1), $(NH_4)_2PtCl_4$ (2), and Na_2PtCl_6 (3). (Reprinted with permission from reference 15. Copyright 2000, American Chemical Society.)

the ordered structure motifs $\bar{d}$ increases from 2.7 to about 3.4 nm after the addition of the metal compounds (compared to the initial complex), but the parameters describing the degree of order remain practically unchanged. The internal order is even enhanced after the metal reduction with both sluggish and fast reducing agents. The gel–surfactant ordering increases locally during the nanoparticle formation while the volume fraction of the ordered structures in the samples decreases. This indicates that the highly ordered surfactant areas within hydrogels concentrate around the growing nanoparticles. In contrast, when the $PtCl_6^{2-}$ ions are incorporated into the PMA–CPC complex, the ordering changes due to new micellar structures. The latter are formed as a result of the interaction of the $PtCl_6^{2-}$ ions with the cetyl pyridinium cations. The reduction of a metal compound is accompanied by restoration of the initial PMA–CPC ordering; however, an increase of the local ordering similar to the PDADMACl/SDS(SDBS) systems does not occur.

SOFTbank E-Book Center Tehran, Phone: 66403879,66493070 For Educational Use.

TABLE 4.1. Structural Characteristics of the Hydrogel–surfactant Complexes Obtained from the SAXS and ASAXS Data

Sample	s_{max} (nm^{-1})	$\bar{d}$ (nm)	L (nm)	$\Delta/\bar{d}$
	PDADMACl–SDBS			
Collapsed gel	2.34	2.68	27	0.100
Gel + $H_2Pt(OH)_2Cl_4$	1.88	3.34	38	0.094
Gel + $H_2Pt(OH)_2Cl_4$ + $NaBH_4$	1.87	3.36	74	0.066
Gel + $H_2Pt(OH)_2Cl_4$ + N_2H_4	1.94	3.24	60	0.074
	PDADMACl–SDS			
Collapsed gel	1.53	4.10	31	0.116
Gel + H_2PtCl_6	1.52	4.13	29	0.118
Gel + $(NH_4)_2PtCl_4$	1.51	4.17	32	0.114
Gel + Na_2PtCl_6	1.52	4.13	38	0.105
Gel + $H_2Pt(OH)_2Cl_4$	1.58	3.98	39	0.101
Gel + Na_2PtCl_6 + $NaBH_4$	1.56	4.02	98	0.064

Source: Reprinted with permission from reference 15. Copyright 2000, American Chemical Society.

As can be seen from the discussion above, the polyelectrolyte gel–surfactant complexes present interesting hybrid metal–polymer nanocomposites, allowing a vast variety of incorporated metals and metal–polymer–surfactant structures. The limitations of these systems are their heterogeneous character (insoluble in any media) and excessive sensitivity to external parameters (pH, temperature, etc.).

2.2. Hypercrosslinked Polystyrene

Hypercrosslinked polystyrene (HPS) [17, 18] is a unique polymer network consisting of nano-sized rigid cavities (pores) with a size in the 2- to 3-nm range (Figure 4.2). HPS is normally synthesized by incorporating methylene groups between adjacent phenyl rings in a dissolved polystyrene homopolymer or a gelled poly(styrene-*r*-divinylbenzene) copolymer in the presence of ethylene dichloride (a good solvent), yielding a very high degree of crosslinking density (may exceed 100%). HPS is able to swell in a wide variety of different solvents, even thermodynamically poor ones (e.g., water) that facilitate incorporation of various organometallic compounds into the nanostructured HPS matrix. The first use of HPS as a medium for Co nanoparticle formation was reported by us in 1999 [19]. Cobalt nanoparticles have been selected due to the established correlation between size and shape of Co particles and their mag-

SOFTbank E-Book Center Tehran, Phone: 66403879,66493070 For Educational Use.

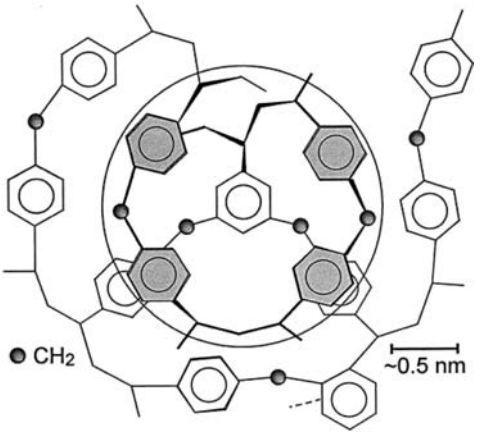

Figure 4.2. Schematic illustration of the internal network of hypercrosslinked polystyrene (HPS). The speckled phenyl rings reside in a different plane relative to the unspeckled ones in the crosslinked material, and each circle identifies a postulated cavity in which Co nanoparticles could grow. (Reprinted with permission from reference 19. Copyright 1999, American Chemical Society.)

netic properties [20]—that is, characteristics of their ferromagnetic resonance (FMR) spectra. Co particles with diameters below 1 nm are nonmagnetic, while the particles with diameters in the range 1–10 nm are superparamagnetic. Larger Co particles are ferromagnetic. In addition, the width of the FMR signal (ΔH) for spherical particles correlates with the size of the Co nanoparticles [20, 21], while the position corresponding to the zero signal (H_0) bears information regarding the shape of the Co nanoparticles. This allows one to determine the general size and shape characteristics of Co nanoparticles solely from FMR spectra.

The Co compounds, $Co_2(CO)_8$ or $[Co(DMF)_6]^{2+}[Co(CO)_4]^-{}_2$ complex, were incorporated in HPS by wet impregnation in 2-propanol or dimethylformamide (DMF), respectively (Table 4.2). The subsequent thermolysis at 200°C results in the formation of Co nanoparticles, the loading and characteristics of which were investigated by X-ray fluorescence (XRF) spectroscopy, FMR spectroscopy, and transmission electron microscopy (TEM). The FMR data presented in Figure 4.3 and Table 4.2 confirmed the formation of spherical nanoparticles [19]. A 2–8 wt. % Co loading the magnitude of the FMR line width indicates that the mean Co nanoparticle diameter is about 2 nm, agreeing well with the mean particle diameter obtained from TEM. When Co content increases above 8 wt. %, the mean particle diameter also increases due to an increase in the population of large Co nanoparticles up to 15 nm in diameter. Here, controlled nanoparticle growth over a wide range of Co contents is

SOFTbank E-Book Center Tehran, Phone: 66403879,66493070 For Educational Use.

TABLE 4.2. FMR Data of HPS–Co Samples Thermolyzed at 200°C and Various Durations

Co Content (wt. %)	Time of Thermolysis (hr)	H_0 (Oe)	ΔH (Oe)
	$Co_2(C0)_8$		
0.9	2	3115	170
0.9	6	3100	250
3.0	2	3040	200
3.0	6	3050	200
3.0	10	3035	200
	$[Co(DMF)_6]^{2+}[Co(CO)_4]_2^-$ in DMF		
1.2	2	3100	200
1.2	6	3050	200
1.2	10	3060	220

Source: Reprinted with permission from reference 19. Copyright 1999, American Chemical Society.

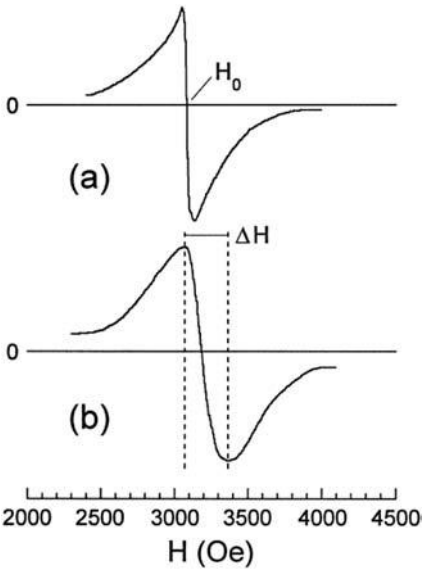

Figure 4.3. FMR spectra of the HPS–Co specimens containing **(a)** 5.07 and **(b)** 10.08 wt. % Co and obtained by thermolysis at 200°C for 2 hr. Labeled in panel **a** is the definition of H_0, the magnitude of which is related to the shape of the Co nanoparticles. The vertical dashed lines in panel **b** identify the line width corresponding to ΔH, which provides a measure of particle size. (Reprinted with permission from reference 19. Copyright 1999, American Chemical Society.)

SOFTbank E-Book Center Tehran, Phone: 66403879,66493070 For Educational Use.

attributed to nanoscale HPS cavities, physically restricting the size of growing particles. It is worth mentioning that the HPS used in this work contains no functional groups, the interaction of which with particle interface might restrict the particle growth and stabilize the particles. Moreover, the nanoscale cavities in HPS are highly interconnected so they should *not* obstruct the migration of Co atoms or even small Co clusters. A steric limitation arising from the predominance of phenyl rings represents the most probable reason for controlled Co nanoparticle growth in HPS; phenyl rings may interact with metal surfaces and nonspecifically stabilize metal nanoparticles. When the Co content in the HPS–Co composite exceeds 10 wt.% (likely a saturation limit), a small fraction of large nanoparticles appears. Their size might correlate with the statistics of the pore size distribution of the HPS matrix.

As can be seen from the above discussion, HPS is a robust, commercially available (by Purolite Int.) nanostructured polymer, yielding control over nanoparticle formation. We believed that this control could be executed for a vast variety of nanoparticles. Following this path, we synthesized Pd and Pt nanoparticles in HPS, using reduction of Pd and Pt compounds instead of thermolysis for the final step of metal–polymer nanocomposite synthesis. Impregnation of HPS with tetrahydrofuran (THF) solution containing platinic acid (H_2PtCl_6) results in the formation of Pt(II) complexes within the nanocavities of HPS [22]. Hydrogen reduction of these metal–polymer nanocomposites yields stable Pt nanoparticles with a mean diameter of 1.3 nm (Figure 4.4). One might recall that for Co-containing HPS, the mean particle size was about 2 nm. This discrepancy in particle size can be explained by different mechanisms of Co and Pt nanoparticle formation. Since Co nanoparticle formation

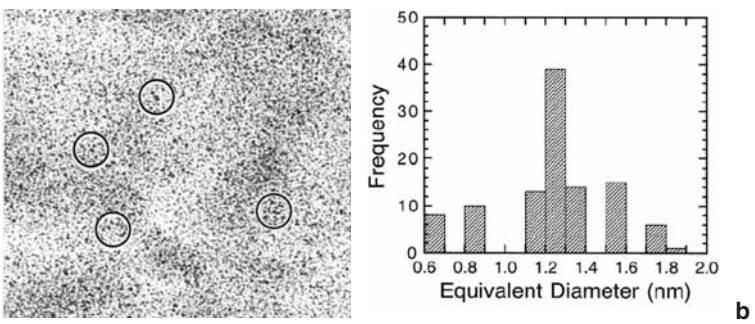

Figure 4.4. Transmission electron micrograph **(a)** and particle size histograms **(b)** of HPS–Pt–THF after H_2 reduction. Groups of single Pt nanoparticles in *a* are highlighted by circles. (Reprinted with permission from reference 22. Copyright 2001, American Chemical Society.)

SOFTbank E-Book Center Tehran, Phone: 66403879,66493070 For Educational Use.

occurs at 200°C, Co clusters could easily migrate between the HPS pores, yielding Co nanoparticles, whose sizes match the pore size. By contrast, H_2 reduction of Pt nanoparticles occurs at a room temperature, and migration of the Pt clusters or atoms or the Pt precursor molecules from pore to pore is unlikely. This results in the formation of Pt nanoparticles, sizes of which correspond to the size of the Pt precursor (salt or complex) filling the pores [22]. Thus, HPS controls the Co nanoparticle size by physical limitation of their growth within the pore ($D = 2$ nm), while for Pt nanoparticles, pores limit the amount of precursor filling the single pore so when the precursor shrinks during reduction due to the increase of the material density (from Pt complex to Pt metal), the Pt nanoparticle occupies a smaller volume. In both cases, HPS provides strong control over nanoparticle growth. The simplicity of this approach and commercial availability of HPS make this polymer system valuable for broader use. However, the drawback of this system is in the crosslinked nature of HPS so no films or coatings can be made, which limits prospects for HPS use in optical or magnetic materials. When HPS is used for heterogeneous catalysis, this limitation becomes an advantage since this catalyst does not require an additional support. Another drawback of the metallated HPS is the easy removal of metal nanoparticles from the polymer in any media where PS swells. To prevent metal loss, HPS-based catalysts should be used only in poor (for PS) solvents (water is the best); thus swelling is minimized.

2.3. Nanocavities in Polyoctadecylsiloxane

To enhance the stability of nanoparticles inside polymer nanocavities, one should use functional polymers providing the functionalization of the nanocavities. As an example, here we discuss polyoctadecylsiloxane (PODS) containing nanocavities formed by a siloxane bilayer [23, 24]. This polymer is obtained by hydrolytic polycondensation of octadecyltrichlorosilane in water. The resultant condensate consists of highly uniform microcrystallites in which the inorganic siloxy backbones form periodic layers, each containing a monomolecular layer of intercalated water, separated by crystalline assemblies of alkyl chains [23]. The siloxy bilayers form nanocavities with surface silanol groups. When this polymer is placed in an aqueous solution of a metal salt (such as K_2PtCl_6, K_2PtCl_4, K_2PdCl_4, etc.), it absorbs the salt into its hydrophilic layer [25, 26]. Subsequent reduction yields regularly spaced metal nanoparticles, as depicted in Figure 4.5. For metallated PODS samples, metal compound loading greatly depends on the compound type. Incorporation of all divalent ions is driven by entropy: Hydrogen bond formation between the chlorine atoms of metal anions and the silanol groups leads to replacement of several water molecules with each $PtCl_4^{2-}$ or $PdCl_4^{2-}$ ion. In so doing, planar ions ($PdCl_4^{2-}$, $PtCl_4^{2-}$) easily penetrate thin siloxy bilayers, while incorporation of bulkier octahedral $PtCl_6^{2-}$

SOFTbank E-Book Center Tehran, Phone: 66403879,66493070 For Educational Use.

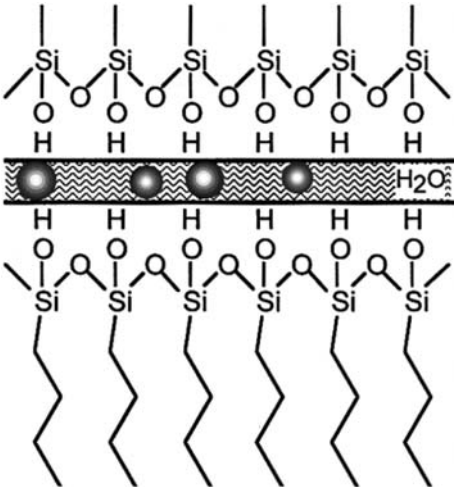

Figure 4.5. Schematic representation of nanoparticle formation in the PODS siloxy bilayer. (Reprinted with permission from reference 25. Copyright 2000, American Chemical Society.)

ions is less successful and the degree of metallation is lower. Reduction of metal compounds with PODS silanol groups (for $PtCl_4^{2-}$) or added reducing agents (for other ions) yields metal nanoparticles located in the siloxy bilayers (Figure 4.6).

As assessed by ASAXS and TEM, in these metal–polymer nanocomposites the particle size distribution is narrow (Figure 4.7) and the metal nanoparticle size does not depend on the reducing agent type, on the metal compound loading, and on the metal compound type. This indicates a "cage" effect, limiting the particle growth by the cavity size. In Figure 4.6 one can see that particles are located solely in the siloxy bilayers. These nanoparticles measure about 1–2 nm in diameter and possess a narrow size distribution likely due to limited volume availability within the siloxy bilayers. Thus, the cavity size of the nanostructured polymer controls the nanoparticle growth. However, the degree of metallation in this material is low due to low fraction of silanol groups. To enhance functionality of PODS's, we impregnated the ordered polymer with surfactants (cetylpyridinium chloride, CPC) or with other long-chain functionalized molecules, incorporation of which inside the PODS hydrocarbon layers was driven by the hydrophobic–hydrophobic interaction in a hydrophilic media (water–ethanol and water–acetone). After this functionalization, we were able to load the hydrophobic layers of the modified PODS's

SOFTbank E-Book Center Tehran, Phone: 66403879,66493070 For Educational Use.

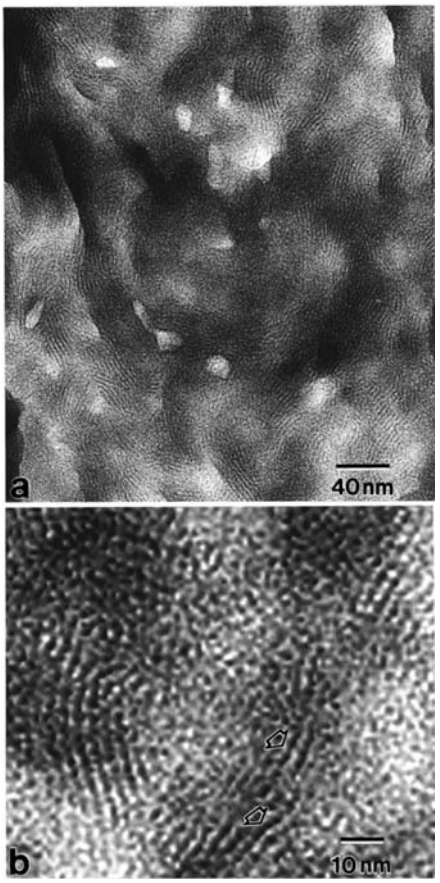

Figure 4.6. **(a)** A TEM image of PODS-Pt1, derived from K_2PtCl_4 and reduced by the silanol groups of PODS. According to elemental analysis, this system contains 1.20 wt. % Pt. **(b)** An enlargement of **(a)** to permit closer examination of the Pt nanoparticles (arrowheads) within the PODS nanostructure. (Reprinted with permission from reference 25. Copyright 2000, American Chemical Society.)

with a higher fraction of metal ions. In so doing, metal nanoparticle formation was not restricted to the siloxy bilayer and was not controlled by cavity size. Thus, PODS allows regular spatial positioning of the nanoparticles and control over the nanopraticle growth (Figure 4.7), but the material is crosslinked and metal loading is low. The functionalization of PODS with functional long-chain hydrocarbons yields a higher degree of metallation, but nanoparticle growth becomes dependent on the reaction conditions (for example, the type of a reducing agent).

SOFTbank E-Book Center Tehran, Phone: 66403879,66493070 For Educational Use.

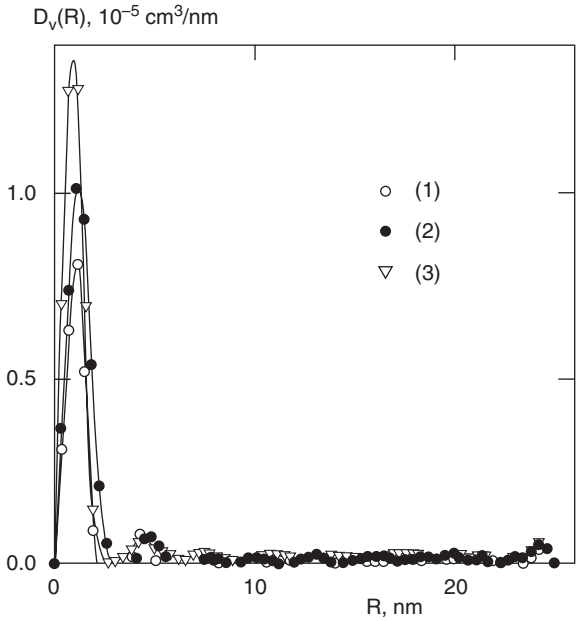

Figure 4.7. Volume distribution functions of the Pt nanoparticles in PODS. Curves 1–3 correspond to the samples based on K_2PtCl_4 after self-reduction and $H_2PtCl_6 \times 6H_2O$ after H_2 and $NaBH_4$ reduction, respectively. (Reprinted with permission from reference 26. Copyright 2000, American Chemical Society.)

3. SOLUBLE POLYMER NANOSTRUCTURES

The existence of nanostructures in polymeric systems assumes the presence of interfaces, so if these systems are solubilized in any solvent without loss of nanostructure (interfaces), they are not genuinely homogeneous, but rather nanoheterogeneous. In this case, interfaces are formed within a nanometer size volume, while these systems are colloidally soluble. Examples of such systems are various kinds of block copolymer micelles, microgels, and polymer colloids.

3.1. Nanoparticles in Block Copolymer Micelles

3.1.1. Cores of Block Copolymer Micelles. In selective solvents (a good solvent *only* for one block), amphiphilic block copolymers form micelles, the characteristics of which (size and shape) depend on the chemical structure and molecular weight of each block and on the solvent type [27–29]. If the core-forming block contains functional groups, which are able to react with metal

SOFTbank E-Book Center Tehran, Phone: 66403879,66493070 For Educational Use.

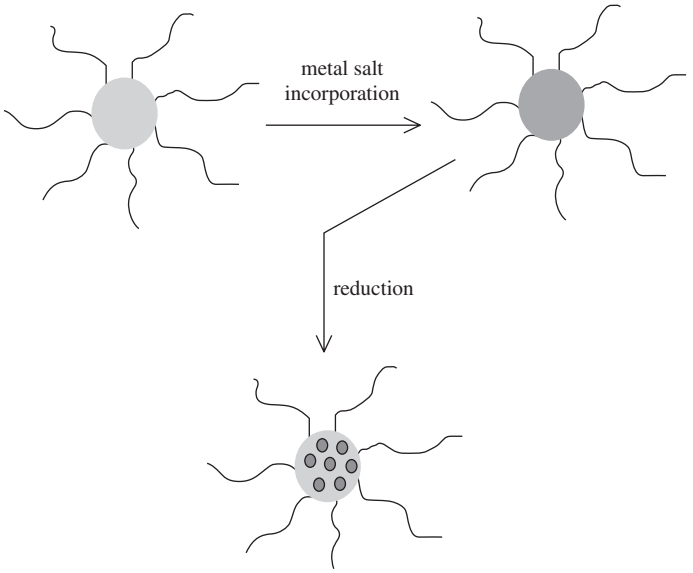

Figure 4.8. Schematic image of metallation of the block copolymer micelle cores.

compounds forming complexes or salts, the micelle core can be charged with a metal compound (Figure 4.8). A block containing no functional groups but providing solubility and micelle stability in a respective solvent should form the micelle corona. Then any further transformations of metal compounds (reduction, thermolysis or other), leading to metal nanoparticle formation, are contained in the core as in a nanoreactor (Figure 4.8). Although micelles are colloidally soluble in the selective solvent, the micelle core can be regarded as quasi-solid, forming the interface between core and corona. In 1995 we described formation of gold nanoparticles in the micelle cores of polystyrene-*block*-poly-4-vinylpyridine (PS-*b*-P4VP) [30]. Practically simultaneously, synthesis of metal and semiconductor nanoparticles in the cores of amphiphilic block copolymer micelles was reported by several research groups [30–35]. As was shown for Au, Pd, and Pt nanoparticles formed in the PS-*b*-P4VP micelles, the nanoparticle morphology strongly depends on the type of reducing agent. A sluggish reducing agent yields one nanoparticle per micelle ("cherry-like" morphology) or a few large particles (Figure 4.9) [35]. If the micelle is crosslinked [36]—that is there is no exchange of macromolecules between micelles—the morphology with a single particle per micelle is feasible. A fast reducing agent yields a so-called "raspberry-like" morphology, containing many small particles per micelle [30]. The latter morphology is thought to be preferable for catalytic applications (Figure 4.9) [35]. In a similar fashion, we

SOFTbank E-Book Center Tehran, Phone: 66403879,66493070 For Educational Use.

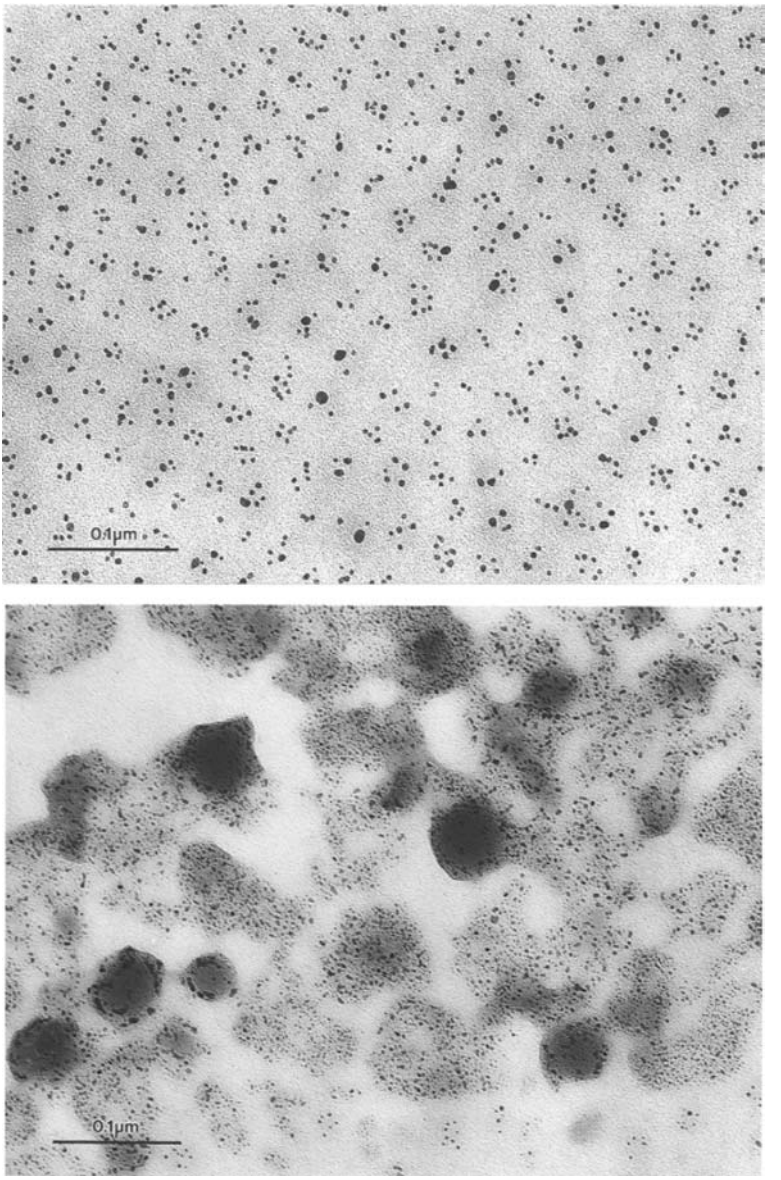

Figure 4.9. Electron micrographs of the Pd colloids synthesized in the PS-*b*-P4VP block copolymer via reduction with hydrazine **(top)** and $NaBH_4$ **(bottom)**. (Reprinted with permission from reference 35. Copyright 1997, American Chemical Society.)

SOFTbank E-Book Center Tehran, Phone: 66403879,66493070 For Educational Use.

have synthesized bimetallic nanoparticles (PdAu, PdPt, and PdZn) in the PS-*b*-P4VP micelles, yet bimetallic particle morphology depends on the metal pair [37]. FTIR spectra of CO adsorbed onto bimetallic nanoparticles demonstrate the presence of solely Pd atoms on the PdAu nanoparticle surface and the existence of a single type of active centers, while the PdPt and PdZn bimetallics display both Pd and Pt (or Zn) atoms on the nanoparticle surface and the presence of two types of active centers on Pd. The Pd monometallic and PdAu, PdPt, and PdZn bimetallic colloids formed in the PS-*b*-P4VP block copolymer micelles were studied in the hydrogenation of dehydrolinalool (DHL) to linalool (a fragrant substance and a precursor of vitamins A, E, and K). The catalytic activities of bimetallic catalysts were found to be higher than that of the Pd nanoparticles due to the modifying influence of the second metal. For all the catalysts, the optimal conditions were found, providing high selectivity of hydrogenation (up to 99.8%), which is most likely determined by the modifying influence of pyridine groups in the P4VP cores.

Similar to noble metal nanoparticles, Co nanoparticles can be prepared by incorporation of $CoCl_2$ (which is almost insoluble in toluene) in the PS-*b*-P2VP micelles followed by reduction. This results in very small spherical particles (below 1 nm in diameter), the thermal treatment of which at 200°C for 2 hr yields spherical nanoparticles with diameters in the range of 3–5 nm [38]. In the solid state these metal–polymer nanocomposites display extraordinarily high magnetization value at comparatively low Co content; that is, we obtained a tenfold increase of the specific magnification density.

Another suitable Co source is $Co_2(CO)_8$. Despite the fact that this compound is well-soluble in toluene, its preferable incorporation into the micelle core occurs due to formation of cationic–anionic complexes involving 4-VP units [38]. The shape and size of the Co nanoparticles formed after thermolysis of the $Co_2(CO)_8$-filled micelles can he controlled by the ratio N/Co and can be varied from the spherical particles (at low Co loadings) to a star-like and cubic morphology at higher $Co_2(CO)_8$ loading [38]. In this case, both superparamagnetic and ferromagnetic nanocomposites can be obtained. The coercive force for the latter varies from 250 to 450 Oe, depending on the Co content and block ratio.

Recently, block copolymers micelles filled with MoS_x nanoparticles (well miscible with mineral oil) were synthesized in heptane using interaction of $Mo(CO)_6$ with polystyrene-*block*-polybutadiene (PS-*b*-PB) and polystyrene-*block*-polyisobutylene (PS-*b*-PIB) followed by H_2S treatment [39]. To position MoS_x nanoparticles in the PS core, the reaction between $Mo(CO)_6$ and block copolymer should be carried out in argon atmosphere. This yields arene Mo tricarbonyl complexes while olefin Mo carbonyl complexes do not form. By contrast, to place MoS_x nanoparticles in the PB corona, complexation with $Mo(CO)_6$ should be carried out in the CO atmosphere. This suppresses forma-

SOFTbank E-Book Center Tehran, Phone: 66403879,66493070 For Educational Use.

tion of arene $Mo(CO)_3$ complexes and ensures oleftin $Mo(CO)_x$ complexes in the PB corona. MoS_x composition can be influenced by varying the sulfiding temperature: Increase of sulfiding temperature to 98°C results in the species whose elemental analysis matches to MoS_3 or MoS_2. At all compositions, MoS_x nanoparticles are amorphous even when the nanoparticle diameter reaches 4.5 nm. For the PS-*b*-PB block copolymer, the location of MoS_x species in the micelle corona makes them more accessible to working surfaces and allows better antifrictional properties than those for MoS_x species situated in the micelle core. By contrast, for PS-*b*-PIB, whose overall micelle density is low, location of MoS_x nanoparticles in the micelle core also leads to a low friction coefficient and a high critical load. On top of that, addition of block copolymer micelles filled with MoS_x nanoparticles improves antiwear properties. These characteristics make block copolymer micelles filled with MoS_x nanoparticles, prospective additives to lubricating oils.

Among all the block copolymers, forming micelles in organic solvents, PS-*b*-P4VP is the most versatile one, since interaction of pyridine units with nearly any metal compound is feasible. In addition, metallated block copolymer micelles are very stable in toluene solutions (for months and years); this often makes PS-*b*-P4VP a polymer of choice. However, from the environmental point of view, one would prefer using less hazardous solvents and water is a preferred solvent. However, when water is concerned as a solvent, there are very few suitable block copolymers—that is, those forming micelles in water and containing functional groups in the micelle core. A few examples of such block copolymers include PEO-*b*-P2VP and PEO-*b*-PB [40, 41]; the micellization of the former block copolymer depends on pH [42]. At pH below 5, PFO-*b*-P2VP becomes molecularly soluble in water. However, if a metal compound is already incorporated into the P2VP core, lowering the pH of the PEO-*b*-P2VP micellar solution does not lead to the micelle decomposition: Coordination with the metal compound keeps micelles intact. Despite the fact that all metal salts studied are soluble in water, the metal compound was found to be completely bound to the micelle cores as shown by ultracentrifugation [40]. The driving force for interaction with a metal compound and the rate of a metal uptake depend on the type of the metal salt. Cations (Pd^{2+}) coordinate directly with the pyridine units of the core-forming block, and this process is completed within 15 min. In the case of salts containing the noble metal in the anion (Na_2PtCl_6, Na_2PtCl_4, Na_2PdCl_4), the interaction of micelles with metal salts takes place due to ligand exchange of Cl^- for pyridine units, and this process can require days. Protonation of P2VP units either by preliminary acidification with HCl followed by addition of a neutral metal compound or by using metal-containing acids (such as H_2PtCl_6 or $HAuCl_4$) yields immediate metal binding and micelle formation due to electrostatic interaction and hydrogen bonding. Although the salt is immediately bound, structural equilibration of such micelles demands longer

SOFTbank E-Book Center Tehran, Phone: 66403879,66493070 For Educational Use.

times. Reduction of the metal ions embedded in the PEO-*b*-P2VP micelles results in the formation of well-defined noble metal nanoparticles, the size and stability of which depend on the metal loading and on the micelle structure. The higher the micelle core density, the larger the particles (if all othet condition are identical), suggesting that the nanoparticle size depends on a local metal concentration while diffusion limitations of metal ions are not crucial.

Palladium nanoparticles formed in PEO-*b*-P2VP micelles were studied in selective hydrogenation of DHL to linalool by varying solvent composition ("isopropanol : water" ratio) and the pH of the reaction medium [43]. As was established with TEM and AFM, isopropanol fraction and KOH loading control the micellar characteristics, which in turn govern the catalytic properties. The larger and denser the micelles, the slower the reaction due to internal diffusion limitations within the micelles. At the same time, denser micelle cores provide better modification of the Pd nanoparticle surface with pyridine units and higher selectivity. The highest selectivity (99.4%) was obtained at pH of 9.4 and 95 vol. % of isopropanol. The highest observed TOF (turnover frequency) value was found to be 24.4 sec^{-1} at pH of 13.0 and 70 vol. % of isopropanol.

Unlike PEO-*b*-P2VP, the PEO-*b*-PB block copolymer micelles in water are very dense, so they successfully fulfill two roles: They serve as nanoreactors for Pd, Pt, and Rh nanoparticle formation and as metal-particle-containing templates for mesoporous silica casting [41]. Figure 4.10 presents PEO-*b*-PB micelles (M^{PB} = 13,400; M^{PEO} = 19,200) filled with Pd nanoparticles and mesoporous silica cast over this block copolymer template. Variation of block lengths and composition of the PEO-*b*-PB block copolymers enables the adjustment of the pore size and pore structure of mesoporous silica along with the simultaneous size control of metal nanoparticles. By varying the metal compound type or the way of metal particle formation and treatment, we were able to influence the metal particle size and particle size distribution. It is believed that any amphiphilic block copolymers, forming dense, functionalized micelles in water, can be used for templating of mesoporous metal oxides with metal nanoparticles.

3.1.2. Coronas of Block Copolymer Micelles. If the nanoparticles are synthesized in the corona of amphiphilic block copolymer micelles, they might be more accessible to the substrate in catalytic reactions and become more efficient catalysts. However, synthesis of nanoparticles in the micelle corona is not straightforward. If the micelle corona contains functional groups able to interact with metal compounds, these micelles will precipitate during complexation. If the micelle corona is not functionalized, then nanoparticle stabilization is only governed by hydrophobic interactions with the hydrophobic micelle core, and the stability of the soluble metal–polymer nanocomposites will be inferior [44]. To improve stabilization in the micelle coronas, we suggested using hybrid

SOFTbank E-Book Center Tehran, Phone: 66403879,66493070 For Educational Use.

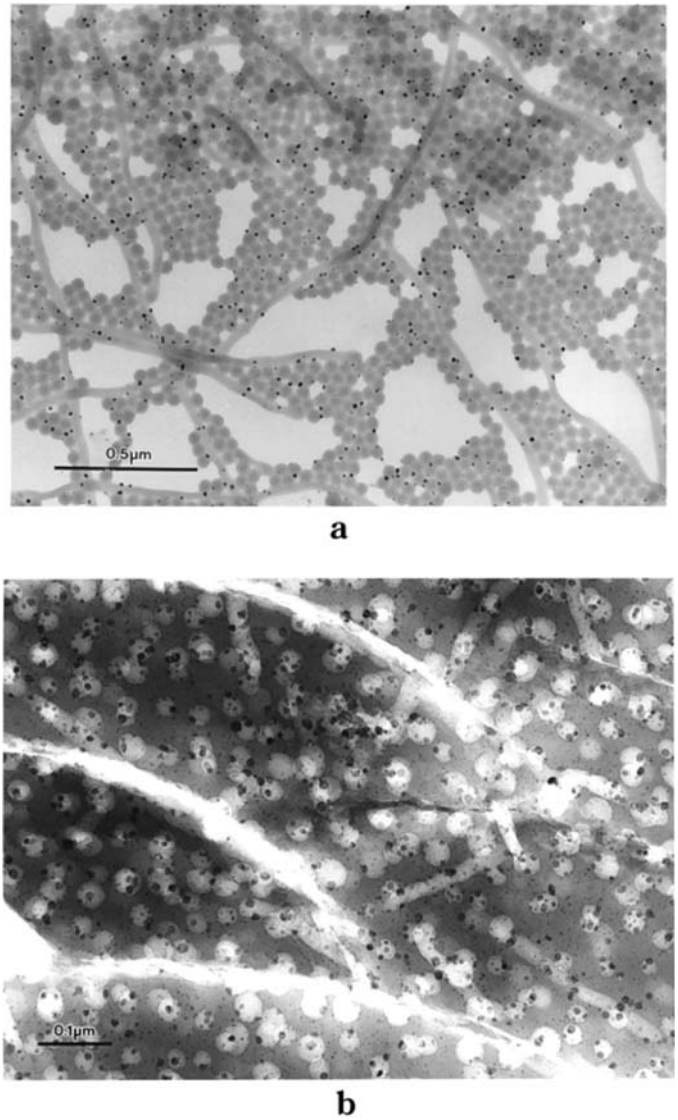

Figure 4.10. TEM images of the Pd colloids formed in the PB-*b*-PEO-I block copolymer micelles **(a)** and mesoporous silica obtained from PB-*b*-PEO-I-Pd(0) as the template after calcination **(b)**. (Reprinted with permission from reference 41. Copyright 1999, American Chemical Society.)

SOFTbank E-Book Center Tehran, Phone: 66403879,66493070 For Educational Use.

micelles consisting of PS-*b*-PEO and cationic or anionic surfactants [45–47]. We assumed that when surfactant is loaded in an aqueous solution containing block copolymer micelles, the favorable path for surfactant molecules will be penetration into the hydrophobic micelle cores. Then surfactant head groups will be located on the core–corona interface or in its vicinity. Ion exchange of surfactant counterions for the ions of choice (Pt, Pd, or Rh) was expected to saturate the corona with the given ions. Combination of dynamic light scattering (DLS), sedimentation in an ultracentrifuge (UC), and ^{1}H NMR spectroscopy allowed us to prove comicellization of block copolymer macromolecules and cationic or anionic surfactants. Ion exchange of the surfactant counterions in the PS-*b*-PEO/CPC system for $PtCl_6^{2-}$ or $PdCl_4^{2-}$ ions followed by reduction of metal-containing hybrid micellar systems (PS-*b*-PEO/CPC/MX_n) with $NaBH_4$ or H_2 yields nanoparticles, the morphology and stability of which depend on the metal compound loading and the type of the reducing agent [45]. $NaBH_4$ reduction leads to decomposition of micellar clusters and formation of micelles with embedded nanoparticles (Figure 4.11). These systems display exceptional stability (for years), if metal salt loading does not exceed 1.24×10^{-2} M. Hydrogen reduction results in metal nanoparticle formation both in micelles and micellar clusters so colloidal solutions are stable at metal salt concentration below 3.36×10^{-3} M (Figure 4.12). Unlike many other systems [30, 40], here the nanoparticle size does not depend on the reducing agent type, but depends on the metal type [45–47]. We surmise that strong interaction of surfactant head

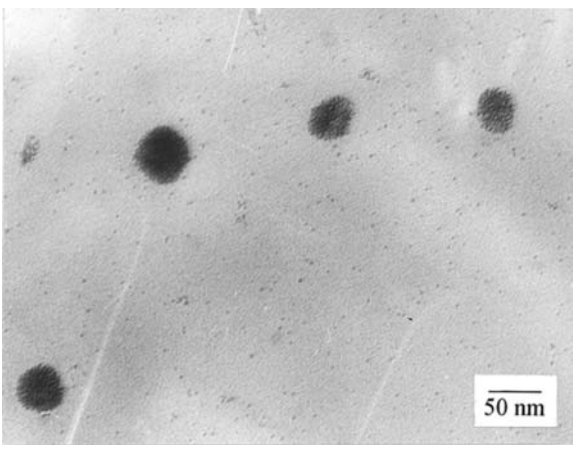

Figure 4.11. TEM micrograph of the Pt nanoparticles stabilized in the PS-*b*-PEO/CPC hybrid micelles in water and obtained via reduction of $H_2PtCl_6 \cdot 6H_2O$ (1.24×10^{-2} mol/L) with $NaBH_4$. (Reprinted with permission from reference 45. Copyright 2000, American Chemical Society.)

SOFTbank E-Book Center Tehran, Phone: 66403879,66493070 For Educational Use.

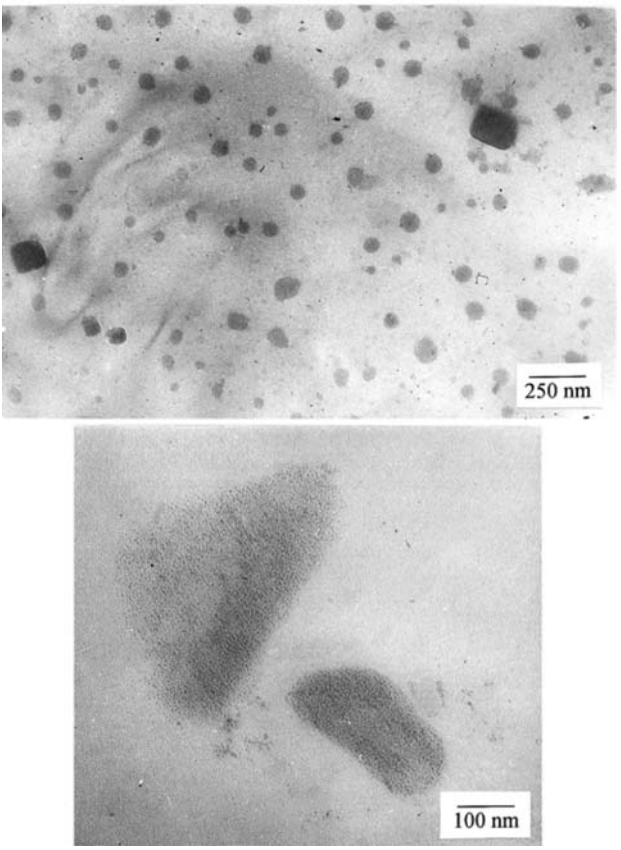

Figure 4.12. TEM micrographs of Pt nanoparticles stabilized in the PS-*b*-PEO/CPC hybrid micelles in water and obtained via reduction of $H_2PtCl_6 \cdot 6H_2O$ (3.36×10^{-3} mol/L) with molecular hydrogen. (Reprinted with permission from reference 45. Copyright 2000, American Chemical Society.)

groups with growing nanoparticles along with hydrophobic interactions with the PS core control the nanoparticle size.

3.1.3. Micelle Formation via Complexation. Micellization of molecularly soluble block copolymers due to interaction with metal compounds was observed in both organic media and water, if one of the two blocks (for a diblock copolymer) is inert while the other is able to form complexes with metal compounds. Micellization of Pd-, Pt-, and Rh-containing polymers derived from PS-*b*-PB with a short PB block was first reported in 1998 [48]. The crosslinks formed due to complexes between metal atoms and PB blocks of different macromolecules were shown to cause micellization. By contrast, Fe carbonyl

SOFTbank E-Book Center Tehran, Phone: 66403879,66493070 For Educational Use.

complexes formed in PS-*b*-PB intramolecularly (no crosslinks) do not yield micelles, and macromolecules remain in the solution. In a similar way, polystyrene-*block*-poly-*m*-vinyltriphenylphosphine (PS-*b*-PPH) was reacted with $(CH_3CN)_2PdCl_2$ or $(PPh_3)_2PdCl_2$ [49]. This resulted in the complexation of triphenylphosphine groups of the PPH block with palladium compounds, inducing micellization instead of gel formation. The morphologies of the Pd-containing PS-*b*-PPH micelles were found to depend on the molecular weight of the diblock copolymer, the block length, and the metal compound type. Interaction of $(CH_3CN)_2PdCl_2$ with PS-*b*-PPH of medium molecular weight (M_w = 29,000) results in the formation of different structures: spherical aggregates, multilamellar vesicles, disklike micelles, and unilamellar vesicles (Figure 4.13) [49]. By contrast, the interaction of $(PPh_3)_2PdCl_2$ with the same block copolymer induces the formation of large multivesicular structures of high uniformity.

The micelles filled with Pd nanoparticles were prepared by reduction of Pd-containing PS-*b*-PPH with $N_2H_4 \times H_2O$, $LiB(C_2H_5)_3H$, or $LiAlH_4$ and analyzed by TEM, X-ray photoelectron spectroscopy (XPS), and X-ray diffraction (XRD) techniques. The size and architecture of Pd nanoparticles formed in the PS-*b*-PPH micellar aggregates was shown to depend on the type of the reducing agent and molecular structure of the Pd complex produced in block copolymer.

In a similar way, micellization via complexation in an aqueous medium was carried out using PEO-*b*-PEI (polyethyeleneimine) [50, 51], since PEI, being a polydentate ligand, easily interacts with any metal compounds yielding metal complexes [52]. Complexation results in aggregation of the PEI blocks and

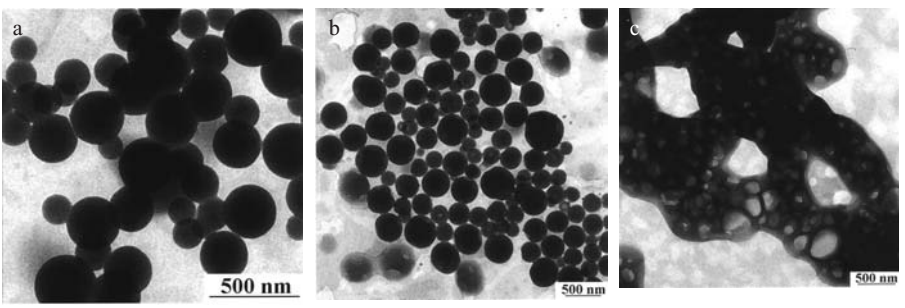

Figure 4.13. **(a)** TEM micrograph of the Pd-containing polymer derived from PS-*b*-PPH1 and $(CH_3CN)_2PdCl_2$. Molar ratio P/Pd = 2/1. **(b)** TEM micrograph of the Pd-containing polymer derived from PS-*b*-PPH1 and $(CH_3CN)_2PdCl_2$. Molar ratio P/Pd = 4/1. **(c)** TEM micrograph of the Pd-containing polymer derived from PS-*b*-PPH1 and $(PPh_3)_2PdCl_2$. Molar ratio P/Pd = 2/1. (Reprinted with permission from reference 49. Copyright 2000, American Chemical Society.)

SOFTbank E-Book Center Tehran, Phone: 66403879,66493070 For Educational Use.

micelle core formation, while PEO blocks form coronas and ensure colloidal solubility. After nanoparticle formation via reduction, PEO-*b*-PEI micelles remain intact, while changing their hydrodynamic parameters. This suggests strong interaction between the PEI units and a metal nanoparticle surface. Similar to amphiphilic block copolymer micelles in selective solvents, the complex-induced micelles also furnish control over nanoparticle nucleation and growth, although micellar and metal particle characteristics are more dependent on the reaction conditions. Since micelle formation is induced solely by complexation with metal compounds, the micelle core densities are low, so the cores here are not quasi-solid any more. Metal nanoparticle morphologies in these systems can be affected in the same way as in amphiphilic block copolymer micelles by varying the reducing agent type, the metal compound loading, and the pH.

3.2. Nanoparticles in Polyelectrolyte Microgels

Polyelectrolyte (PE) microgels are gel spherical particles having diameters in the nanometer range, bearing cationic or anionic groups, and forming colloidal solutions [53, 54]. The microgel stability in the solutions is ensured by crosslinking. Charged groups of PE microgels provide solubilization in water and can be used for ion exchange. When PE microgels are loaded with metals, they can serve as nanoreactors for metal nanoparticle formation. Gold nanoparticles were formed in microgels based on sulfonated PS [55]. Morphologies of nanoparticles are governed by the degree of microgel crosslinking. The higher the crosslinking density, the higher the probability of spherical particles embedded in the microgels. The type of reducing agent is the other key factor. Fast reduction with $NaBH_4$ results in small gold nanoparticles (4.5 nm) located in microgels. When $NaBH_4$ is added in alkaline solution (0.1 N NaOH), the nucleation is slower, resulting in 7-nm nanoparticles forming long "threads." Yet, only 20% of microgels contain nanoparticles; thus, slow nucleation allows Au clusters and ions to migrate out of microgel areas where aggregation easily occurs.

Microgels filled with Pd and Pt nanoparticles have been prepared in a similar way. These microgels were then used as co-templates (along with amphiphilic PS-*b*-PEO block copolymers) for templating of mesoporous silica [56], aluminosilica, and alumina [57]. Here microgels play a dual role: They are nanoreactors for nanoparticle formation and pore-forming templates when mesoporous material is formed. It is noteworthy that aluminas with metal nanoparticles templated both over cationic and anionic microgels consist of an interpenetrating pore system and alumina nanowires (2–3 nm in diameter and about 40 nm in length) along with Pd or Pt nanoparticles (Figure 4.14). This combination yields higher mesoporosity than that of aluminosilicas. Catalytic

SOFTbank E-Book Center Tehran, Phone: 66403879,66493070 For Educational Use.

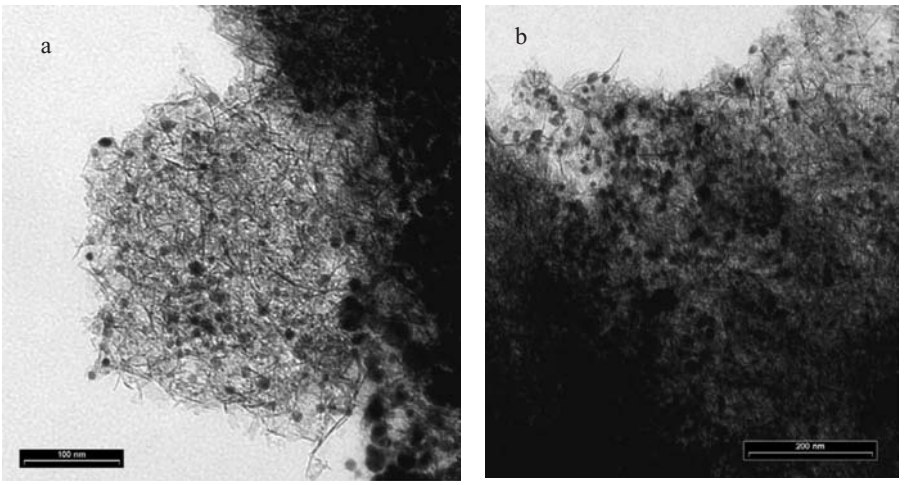

Figure 4.14. TEM images of alumina samples containing Pd nanoparticles and templated over cationic **(a)** and anionic **(b)** microgels. (Reprinted with permission from reference 57. Copyright 2003, American Chemical Society.)

properties of Pd- and Pt-containing aluminosilicas and aluminas were studied in selective hydrogenation of long-chain acetylene alcohols (C_5, C_{10}, C_{20}). Aluminosilica samples showed no appreciable activity or selectivity for either substrate, which is probably caused by high diffusion limitations within pores. Indeed, the shorter the substrate, the higher the activity, so the highest activity was achieved for alcohol C_5. Mesoporous alumina cast over cationic microgels with Pd nanoparticles displayed a high selectivity toward a longest acetylene alcohol C_{20}, along with satisfactory activity. Since normally it is difficult to achieve, we contributed this effect to a perfect correlation between pore, nanoparticle, and substrate sizes.

3.3. Nanoparticles in Multifunctional Polysilsesquioxane Colloids

A new family of polysilsesquioxane colloids was synthesized by hydrolytic condensation of different functional amphiphilic silanes without any additional surfactants [58–60]. To choose a suitable monosubstituted silane, we looked for the combination of a functional group, which would be able to interact with metal compounds, and a hydrophobic part, which would self-assemble in an aqueous medium. We expected that a sol–gel reaction of such a precursor in water would yield multifunctional materials with internal ordering if the hydrophobic tail is sufficiently long. In this way, polysilsesquioxane colloids

SOFTbank E-Book Center Tehran, Phone: 66403879,66493070 For Educational Use.

based on *N*-(6-aminohexyl)aminopropyltrimethoxysilane (AHAPS) were synthesized and studied using SAXS, TEM, liquid- and solid-state NMR, and other methods [58, 59]. Poly-AHAPS (PAHAPS) can be obtained as soluble species (colloids) in water—a poor solvent for AHAPS precursor—or as crosslinked material in THF (a good solvent for AHAPS). Internal lamellar ordering of the AHAPS tails was obtained when the amino groups of the AHAPS molecules were not protonated (no pH adjustment) and aqueous medium was used (Figure 4.15). The size of the PAHAPS colloids depends on the reaction conditions including the dish material where evaporation occurs. Evaporation of a PAHAPS solution on a Teflon dish instead of glass results in much larger colloids because of lack of interaction with the dish surface.

When metal compounds are added to the solution containing PAHAPS colloids, the size of the latter may change, and this change depends on the molar ratio [PAHAPS unit]:metal. For example, when Pt loading is low (40:1), no change (additional aggregation) occurs, while at tenfold increase of the loading, colloid size increases. In so doing, PAHAPS colloid size greatly depends on the Pt compound geometry: A planar $PtCl_4^{2-}$ ion induces higher aggregation during metallation than does an octahedral $PtC1_6^{2-}$ ion. Metal particle formation depends on the metal compound geometry as well [59]. For the planar $PtCl_4^{2-}$ ion (from K_2PtCl_4), metal particle size is determined by the reducing

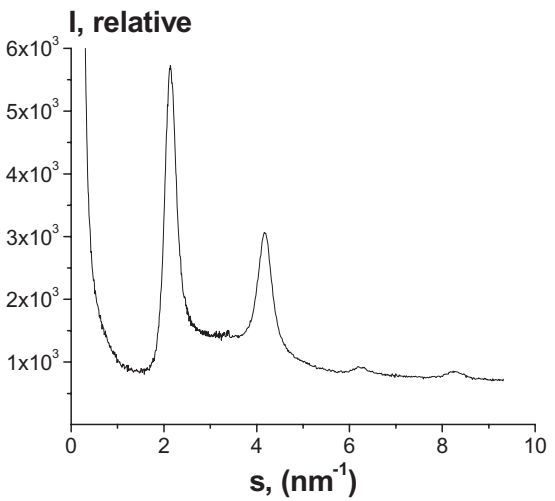

Figure 4.15. SAXS profiles of PAHAPS-H4 in which intensity is shown as a function of scattering vector (s) given by $4\pi \sin(\theta/\lambda)$, where 2θ is the scattering angle and λ (= 0.15 nm) is the wavelength of the incident radiation. (Reprinted with permission from reference 59. Copyright 2003, American Chemical Society.)

SOFTbank E-Book Center Tehran, Phone: 66403879,66493070 For Educational Use.

agent type, while for K_2PtCl_6, particle diameter is fairly independent of the reducing agent (Figure 4.16). However, when H_2PtCl_6 is used, PAHAPS becomes partially protonated and this yields larger particles, although particle size distribution remains very narrow. Since amino groups can interact with the majority of transition-metal compounds, PAHAPS colloids can be used as templates for synthesis of magnetic, semiconductor, metal, or metal oxide nanoparticles with a small variation in the synthetic procedure. A schematic image of PAHAPS metallation is presented in Figure 4.17.

Another interesting feature of these metallated polymer colloids is that they can form dendrites with different size and shape from aqueous solutions containing PAHAPS colloids loaded with metal salts or metal nanoparticles (Figure 4.18) [58]. This phenomenon has been reported for the first time for colloidal polymer particles, although formation of dendrites is common for a number of salts or metals [61, 62]. Because the size and shape of the dendrites can be easily controlled by concentration of polymer solutions and metal loading, metallated PAHAPS may be suggested as catalytically active membranes. This is appropriate in those cases when select surface coverage is important. Another possible application for these dendrites loaded with metal nanoparticles is a conductive layer between two surfaces, as described elsewhere [63] for pure Pd dendrite crystals. Unlike pure metals, advantages of metal-loaded PAHAPS are the lower cost and the greater structural stability.

Polymer colloids with ordered interior were synthesized by sol–gel reaction of octadecyldimethyl(3-trimethoxysilylpropyl)ammonium chloride (ODMACl) and a mixture of ODMACl and the trisodium salt of the triacetic acid *N*-(trimethoxysilylpropyl)ethylenediamine (TANED) [60]. The structure and morphology of these colloids were studied with SAXS, TEM, NMR, sedimentation in ultracentrifuge, and other methods. When polymer colloids are obtained from a single precursor (ODMACl), their local structure, molecular weight characteristics, and morphology greatly depend on the pH value and on the sequence of pH adjustment, while lamellar ordering remains nearly unaffected with Bragg spacing d of about 3.6 nm. This Bragg spacing is significantly smaller than two layers of extended ODMACl tails, so one can assume either tilting of ODMACl chains (they are not perpendicular to the lamellar surface) or intercalation of the tails of the two layers (or both). As we observed no vesicles and the PODMACl colloids are much larger than twice the d spacing, they should have a multilamellar structure.

Hydrolytic condensation of an equimolar mixture of cationic and anionic silanes (ODMACl and TANED) yields zwitterionic copolymer colloids with two-dimensional hexagonal packing. Interaction of the ODMACl quaternary ammonium groups with the three carboxy groups of TANED leads to replacement of sodium and chloride ions and formation of gegenions, resulting in a molar ratio ODMACl : TANED = 3 : 1 (each TANED molecule contains three

SOFTbank E-Book Center Tehran, Phone: 66403879,66493070 For Educational Use.

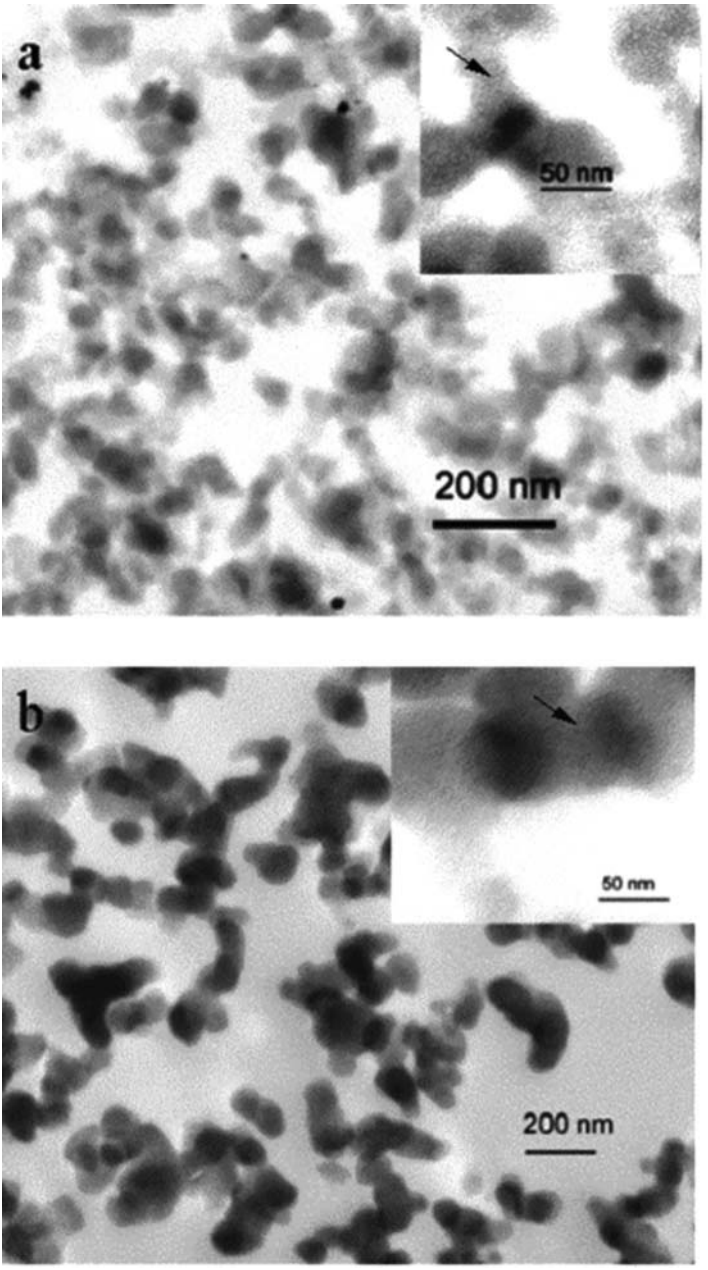

Figure 4.16. TEM images of PAHAPS-F1 colloids prepared by interaction with K_2PtCl_6 at molar ratio [PAHAPS]:Pt = 4:1 followed with $N_2H_4 \times H_2O$ **(a)** or $NaBH_4$ **(b)** reduction. Pt nanoparticles appear like dark dots and are shown by arrows. (Reprinted with permission from reference 59. Copyright 2003, American Chemical Society.)

SOFTbank E-Book Center Tehran, Phone: 66403879,66493070 For Educational Use.

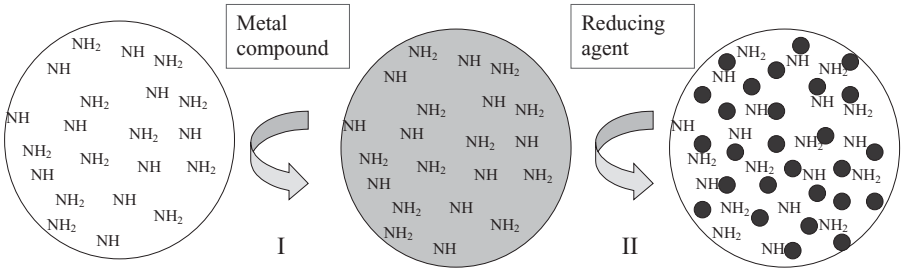

Figure 4.17. Schematic image of PAHAPS colloid metallation. Step I is incorporation of metal compounds inside the PAHAPS colloids due to interaction with amino groups. Step II is metal particle formation due to reduction of metal species. (Reprinted with permission from reference 59. Copyright 2003, American Chemical Society.)

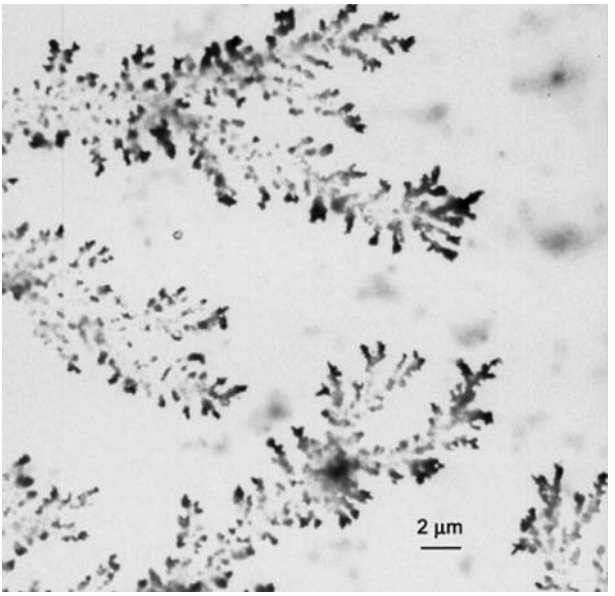

Figure 4.18. TEM image of dendrites formed by PAHAPS colloids containing Pd nanoparticles.

carboxy groups) nearly independently of the initial ODMACl : TANED ratio in the reaction medium. Due to their ordered interior, PolyODMACl (PODMACl) and PODMACl–TANED colloids can be used as templates for controlled positioning of nanoparticles within these colloids. Indeed, since lamellar ordering is preserved during metal reduction, it controls Pt nanoparticle formation within PODMACl colloids providing Pt nanoparticle alignment within the lamellar

SOFTbank E-Book Center Tehran, Phone: 66403879,66493070 For Educational Use.

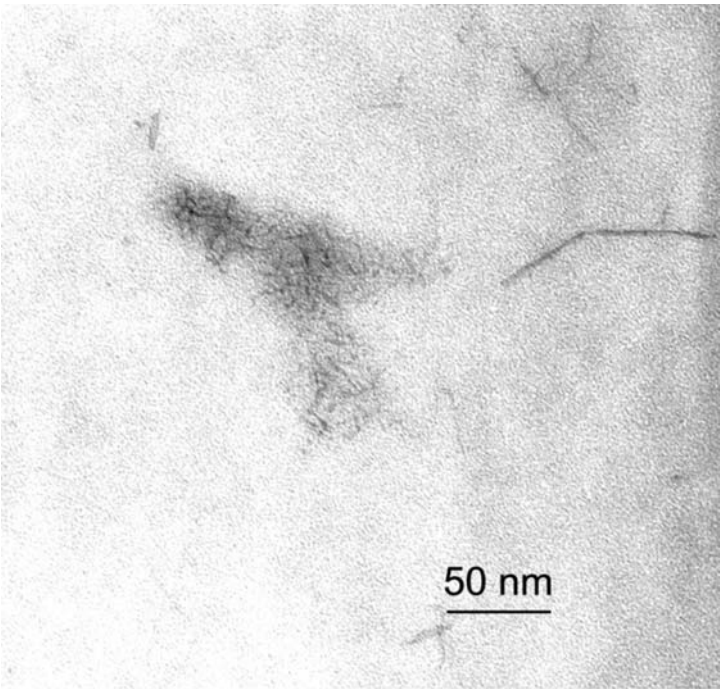

Figure 4.19. TEM image of PODMACl–TANED colloids filled with iron oxide nanoparticles.

structure. Loading of PODMACl–TANED colloids with iron salts followed by pH increase results in the formation of iron oxide nanoparticles located within PODMACl–TANED cylinders (Figure 4.19). This suggests new opportunities for aligning nanoparticles derived from different metal, metal oxides, or semiconductors within ordered polymeric colloids. These materials can be promising for tailoring optical, magnetic, and electric properties of metal nanocomposites by regular positioning of the nanoparticles.

4. CONCLUSIONS AND OUTLOOK

This chapter illustrates our approaches in the design of metal nanocomposites, both in bulk and in solution. The key advantages of soluble systems, especially if they retain solubility after nanoparticle formation, are their potential use for microheterogeneous catalysis and magnetic liquids or formation of thin deposited or free-standing films (the latter were obtained with block copolymer micelles and some functional polysilsesquioxane colloids). These opportunities

SOFTbank E-Book Center Tehran, Phone: 66403879,66493070 For Educational Use.

make promising a number of important applications for nanolithography and catalysis in optical and magnetic materials. On the other hand, for catalytic applications, insoluble metal nanocomposites are often favored, because they do not require an additional support in heterogeneous catalysis. It is noteworthy that the nanoparticle properties can be greatly influenced by designing the polymer nanoenvironment via modification of the nanoparticle surface with polymer functional groups. Hence, the choice of the polymer type and the internal ordering of the nanostructured polymer play a crucial role in the material properties and should be taken into consideration for a specific material application.

Varying the polymer type and characteristics allows development of sophisticated metal–polymer nanocomposites with tunable properties and promise for future applications. Yet, one can expect vigorous development of this field for years to come so that new polymeric systems yielding better control over nanoparticle formation and properties will be designed.

REFERENCES

1. W. Heffels, J. Friedrich, C. Darribere, J. Teisen, K. Interewicz, C. Bastiaansen, W. Caseri, and P. Smith, *Rec. Res. Dev. Macromol. Res.* **2**, 143 (1977).
2. M. W. Ellsworth and D. L. Gin, *Polym. News* **24**, 331 (1999).
3. R. Gangopadhyay and A. De, *Chem. Mater.* **12**, 608 (2000).
4. G. Carotenuto and L. Nicolais, *Rec. Res. Dev. Mater. Sci.* **3**, 303 (2002).
5. C. Sanchez, G. J. de Soler-Illia, F. Rihot, T. Lalot, C. R. Mayer, and V. Cabuil, *Chem. Mater.* **13**, 3061 (2001).
6. V. Sankaran, C. C. Cummins, R. R. Schrock, R. E. Cohen, and R. J. Silbey, *J. Am. Chem. Soc.* **112**, 6858 (1990).
7. M. W. Ellsworth and D. L. Gin, *Polym. News* **24**, 331 (1999).
8. F. Yeh, E. L. Sokolov, A. R. Khokhlov, and B. Chu, *J. Am. Chem. Soc.* **118**, 6615 (1996).
9. A. R. Khokhlov, S. G. Starodubtsev, and V. V. Vasilevskaya, *Adv. Polym. Sci.* **109**, 123 (1993).
10. A. R. Khokhlov, E. Y. Kramarenko, E. E. Makhaeva, and S. G. Starodubtsev, *Macromol. Theory Simul* **1**, 105 (1992).
11. Y. V. Khandurina, A. T. Dembo, V. B. Rogacheva, A. B. Zezin, and V. A. Kabanov, *Vysokomol. Soedin., Ser. A Ser. B* **36**, 235 (1994).
12. H. Okuzaki and Y. Osada, *Macromolecules* **28**, 380 (1995).
13. L. M. Bronstein, O. A. Platonova, A. N. Yakunin, I. M. Yanovskaya, P. M. Valetsky, A. T. Dembo, E. E. Makhaeva, A. V. Mironov, and A. R. Khokhlov, *Langmuir* **14**, 252 (1998).

SOFTbank E-Book Center Tehran, Phone: 66403879,66493070 For Educational Use.

14. L. M. Bronstein, O. A. Platonova, A. N. Yakunin, I. M. Yanovskaya, P. M. Valetsky, A. T. Dembo, E. S. Obolonkova, E. E. Makhaeva, A. V. Mironov, and A. R. Khokhlov, *Colloids Surf A* **147**, 221 (1999).
15. D. I. Svergun, E. V. Shtykova, M. B. Kozin, V. V. Volkov, A. T. Dembo, E. V. J. Shtykova, L. M. Bronstein, O. A. Platonova, A. N. Yakunin, P. M. Valetsky, and A. R. Khokhlov, *J. Phys. Chem. B.* **104**, 5242 (2000).
16. L. M. Bronstein, D. I. Svergun, and A. R. Khokhlov, in *Polymer Gels and Networks*, edited by Y. Osada and A. R. Khokhlov, Marcel Dekker, New York, (2002), p. 103.
17. V. A. Davankov and M. P. Tsyurupa, *React. Polym.* **13**, 27 (1990).
18. M. P. Tsyurupa and V. A. Davankov, *J. Polym. Sci. Polym. Chem. Ed.* **18**, 1399 (1980).
19. S. N. Sidorov, L. M. Bronstein, V. A. Davankov, M. P. Tsyurupa, S. P. Solodovnikov, P. M. Valetsky, E. A. Wilder, and R. J. Spontak, *Chem. Mater.* **11**, 3210 (1999).
20. S. V. Vonsovskii, *Magnetism,* Nauka, Moscow, 1971.
21. C. P. Bean, J. D. Livingston, and P. S. Rodbell, *Acta Metall* **5**, 682 (1957).
22. S. N. Sidorov, I. V. Volkov, V. A. Davankov, M. P. Tsyurupa, P. M. Valetsky, L. M. Bronstein, R. Karlinsey, J. W. Zwanziger, V. G. Matveeva, E. M. Sulman, N. V. Lakina, E. A. Wilder, and R. J. Spontak, *J. Am. Chem. Soc.* **123**, 10502 (2001).
23. A. N. Parikh, M. A. Schivley, E. Koo, K. Seshadri, D. Aurentz, K. Mueller, and D. L. Allara, *J. Am. Chem. Soc.* **119**, 3135 (1997).
24. W. R. Thompson and J. E. Pemberton, *Langmuir* **11**, 1720 (1995).
25. L. M. Bronstein, D. M. Chernyshov, P. M. Valetsky, E. A. Wilder, and R. J. Spontak, *Langmuir* **16**, 8221 (2000).
26. D. I. Svergun, M. B. Kozin, P. V. Konarev, E. V. Shtykova, V. V. Volkov, D. M. Chernyshov, P. M. Valetsky, and L. M. Bronstein, *Chem. Mater.* **12**, 3552 (2000).
27. I. U. Hamley, *The Physics of Block Copolymers*, Oxford University Press, Oxford, UK (1998).
28. S. Förster and M. Antonietti, *Adv. Mater.* **10**, 195 (1998).
29. N. Hadjichristidis, S. Pispas, and G. A. Floudas, *Block Copolymers Synthetic Strategies, Physical Propertie, and Applications*, John Wiley & Sons, Hoboken, NJ (2003).
30. M. Antonietti, E. Wenz, L. Bronstein, and M. Seregina, *Adv. Mater.* **7**, 1000 (1995).
31. M. Antonietti and S. Henz, *Nachr. Chem. Technol. Lab.* **40**, 308 (1992).
32. H. Saito, S. Okamura, and K. Ishizu, *Polymer* **33**, 1099 (1992).
33. M. Moffitt, L. McMahon, V. Pessel, and A. Eisenberg, *Chem. Mater.* **7**, 1185 (1995).
34. J. P. Spatz, A. Roescher, and M. Möller, *Adv. Mater.* **8**, 337 (1996).
35. M. V. Seregina, L. M. Bronstein, O. A. Platonova, D. M. Chernyshov, P. M. Valetsky, J. Hartmann, E. Wenz, and M. Antonietti, *Chem. Mater.* **9**, 923 (1997).
36. L. Bronstein, M. Antonietti, and P. Valetsky, in *Nanoparticles and Nanostructured Films*, edited by J. H. Fendler, Wiley-VCH Verlag: Weinheim, (1998), p. 145.

SOFTbank E-Book Center Tehran, Phone: 66403879,66493070 For Educational Use.

37. L. M. Bronstein, D. M. Chernyshov, I. O. Volkov, M. G. Ezernitskaya, P. M. Valetsky, V. G. Matveeva, and E. M. Sulman, *J. Catal.* **196**, 302 (2000).
38. O. A. Platonova, L. M. Bronstein, S. P. Solodovnikov, I. M. Yanovskaya, E. S. Obolonkova, P. M. Valetsky, E. Wenz, and M. Antonietti, *Colloid Polym. Sci.* **275**, 426 (1997).
39. T. P. Loginova, Y. A. Kabachii, S. N. Sidorov, D. N. Zhirov, P. M. Valetsky, M. G. Ezernitskaya, L. V. Dybrovina, T. P. Bragina, O. L. Lependina, B. Stein, and L. M. Bronstein, *Chem. Mater.* 2003, *submitted.*
40. L. M. Bronstein, S. N. Sidorov, P. M. Valetsky, J. Hartmann, H. Coelfen, and M. Antonietti, *Langmuir* **15**, 6256 (1999).
41. L. Bronstein, E. Kraemer, B. Berton, C. Burger, S. Foerster, and M. Antonietti, *Chem. Mater.* **11**, 1402 (1999).
42. T. J. Martin, K. Prochazka, P. Munk, and S. E. Webber, *Macromolecules* **29**, 6071 (1996).
43. N. V. Semagina, A. V. Bykov, E. M. Sulman, V. G. Matveeva, S. N. Sidorov, L. V. Dubrovina, P. M. Valetsky, O. I. Kiselyova, A. R. Khokhlov, B. Stein, and L. M. Bronstein, *J. Mol. Cat. A: Chem.* (2003).
44. A. B. R. Mayer, J. E. Mark, and R. E. Morris, *Polym. J.* **30**, 197 (1998).
45. L. M. Bronstein, D. M. Chernyshov, G. I. Timofeeva, L. V. Dubrovina, P. M. Valetsky, E. S. Obolonkova, and A. R. Khokhlov, *Langmuir* **16**, 3626 (2000).
46. L. M. Bronstein, D. M. Chernyshov, G. I. Timofeeva, L. V. Dubrovina, P. M. Valetsky, and A. R. Khokhlov, *J. Colloid Interface Sci.* **230**, 140 (2000).
47. L. M. Bronstein, D. M. Chernyshov, E. Vorontsov, G. I. Timofeeva, L. V. Dubrovina, P. M. Valetsky, S. Kazakov, and A. R. Khokhlov, *J. Phys. Chem. B* **105**, 9077 (2001).
48. L. M. Bronstein, M. V. Seregina, O. A. Platonova, Y. A. Kabachii, D. M. Chernyshov, M. G. Ezernitskaya, L. V. Dubrovina, T. P. Bragina, and P. M. Valetsky, *Macromol. Chem. Phys.* **199**, 1357 (1998).
49. D. M. Chernyshov, L. M. Bronstein, H. Boerner, B. Berton, and M. Antonietti, *Chem. Mater.* **12**, 114 (2000).
50. L. M. Bronstein, S. N. Sidorov, A. Y. Gourkova, P. M. Valetsky, J. Hartmann, M. Breulmann, H. Colfen, and M. Antonietti, *Inorg. Chim. Acta* **280**, 348 (1998).
51. S. N. Sidorov, L. M. Bronstein, P. M. Valetsky, J. Hartmann, H. Colfen, H. Schnablegger, and M. Antonietti, *J. Colloid Interface Sci.* **212**, 197 (1999).
52. M. Michaelis and A. Henglein, *J. Phys. Chem.* **96**, 4719 (1992).
53. M. Antonietti, *Angew. Chem.* **100**, 1813 (1988).
54. M. Antonietti, W. Bremser, and M. Schmidt, *Macromolecules* **23**, 3796 (1990).
55. M. Antonietti, F. Gröhn, J. Hartmann, and L. Bronstein, *Angew. Chem. Int. Ed.* **36**, 2080 (1997).
56. N. T. Whilton, B. Berton, L. Bronstein, H.-P. Hentze, and M. Antonietti, *Adv. Mater.* **11**, 1014 (1999).

SOFTbank E-Book Center Tehran, Phone: 66403879,66493070 For Educational Use.

57. L. M. Bronstein, D. M. Chernyshov, R. Karlinsey, J. W. Zwanziger, V. G. Matveeva, E. M. Sulman, G. N. Demidenko, H.-P. Hentze, and M. Antonietti, *Chem. Mater.* **15**, 2623 (2003).
58. L. M. Bronstein, C. Linton, R. Karlinsey, B. Stein, D. I. Svergun, J. W. Zwanziger, and R. J. Spontak, *Nano Lett.* **2**, 873 (2002).
59. L. M. Bronstein, C. Linton, R. Karlinsey, E. Ashcraft, B. Stein, D. I. Svergun, M. Kozin, I. A. Khotina, R. J. Spontak, U. Werner-Zwanziger, and J. W. Zwanziger, *Langmuir* **19**, 7071 (2003).
60. L. M. Bronstein, C. Linton, R. Karlinsey, B. Stein, G. I. Timofeeva, D. I. Svergtun, P. I. Konarev, M. Kozin, J. Tomaszewski, U. Werner-Zwanziger, and J. W. Zwanziger, *Langmuir* **20**, 1100 (2004).
61. H. Honjo and S. Ohta, *Phys. Rev. A* **45**, R8332 (1992).
62. H. C. Zeng and L. C. Lim, *J. Mater. Res.* **13**, 1426 (1998).
63. W. E. Bernier and E. G. Bundga, US 6331119.

SOFTbank E-Book Center Tehran, Phone: 66403879,66493070 For Educational Use.